PHILOSOPHICAL TRANSACTIONS OF THE ROYAL SOCIETY A MATHEMATICAL, PHYSICAL & ENGINEERING SCIENCES

A Study of Unsteady Forces at Low Reynolds Number: A Strong Interaction Theory for the Coaxial Settling of Three or More Spheres

S. Leichtberg, S. Weinbaum, R. Pfeffer and M. J. Gluckman

Phil. Trans. R. Soc. Lond. A 1976 **282**, 585-610
doi: 10.1098/rsta.1976.0065

A STUDY OF UNSTEADY FORCES AT LOW REYNOLDS NUMBER: A STRONG INTERACTION THEORY FOR THE COAXIAL SETTLING OF THREE OR MORE SPHERES

By S. LEICHTBERG,† S. WEINBAUM, R. PFEFFER and M. J. GLUCKMAN

The City College of The City University of New York

(*Communicated by K. Stewartson, F.R.S. – Received* 22 *May* 1975 – *Revised* 12 *January* 1976)

CONTENTS

Unsteady multiparticle creeping motions are complicated by the appearance of Basset, virtual mass and acceleration forces and by the difficulty of calculating fluid–particle interactions for three or more closely spaced particles. The present theoretical and experimental investigation explores the importance of each of these complicating features by examining in detail the gravitational–hydrodynamical interaction between three or more spheres falling along a common axis. The strong interaction theory developed to describe this motion accurately satisfies the viscous boundary conditions along the surface of each sphere and includes all the unsteady force terms in the equations of motion for the spheres. The experimental measurements for the three-sphere chain are in excellent agreement with theoretical predictions provided the Basset force

† Present address: Pratt & Whitney Aircraft, East Hartford, Conn., U.S.A.

is retained in the dynamic force balance. These results indicate, in general, that the Basset force is the most important unsteady force in gravitational flows at low Reynolds numbers in which the flow configuration is slowly changing due to fluid–particle interactions. The unsteady theory for small but finite Reynolds numbers shows that the departures in particle spacings, due to the integrated effect of the Basset force, from those predicted by quasi-steady zero Reynolds number theory grow as $t^{\frac{1}{2}}$ for large times and are of the order of the particle dimensions if the duration of the interaction is of $O(\mathrm{Re}_\infty^{-1} a/U_t)$. Here Re_∞ is based on the terminal settling velocity U_t and radius a of the sphere. This condition is satisfied in most sedimentation problems of interest. Virtual mass and particle acceleration forces on the other hand, are of negligible importance except during a short-lived initial transient period. An intriguing new feature of the three-sphere motion for large times was discovered. One finds that there is a critical initial spacing criterion which determines whether the two leading spheres in the chain will asymptotically approach a zero or a finite fluid gap as time goes to infinity. Numerical solutions for longer chains show that there is a tendency for the leading third of the chain to break up into doublets and triplets whereas the spheres in the latter third of the chain tend to space out separately.

1. Introduction

The motion of particles at low Reynolds number through fluid media under the action of gravitational forces, hydrodynamic interactions, or a combination of both, is important in the mechanics of aerosols and suspensions, and various bio-mechanical applications, e.g. the axial clustering of red blood cells in the microcirculation, Leichtberg, Weinbaum & Pfeffer (1976*b*).

Existing theoretical analyses of the behaviour of finite clusters of particles in unbounded creeping flow have been confined largely to various two-sphere configurations or larger dilute systems where particle interactions are weak. The stimulus for much of the work on two spheres is the well known exact solution by Stimson & Jeffery (1926). Experimental investigations of the two-sphere problem by Bart (1959) and Happel & Pfeffer (1960) have shown excellent agreement with the theoretical results at low Reynolds numbers ($\mathrm{Re} < 0.1$).

The related problem of the interaction of three or more spheres has received much less attention. One interesting study is that of Hocking (1964) for three spheres falling side by side. The analysis is based on a quasi-steady first order reflexion theory and is thus restricted to large sphere spacings. The fundamental difference between particle interactions involving two and three or more identical spheres at very low Re is that the flow configuration for the two-sphere geometry does not change with time since the drag on each sphere is the same. In contrast, three or more spheres have no steady state configuration since multiparticle interaction effects continually change as a function of particle spacing and velocity.

Perhaps the simplest three-sphere strong interaction problem that can be examined both theoretically and experimentally is the axial settling of three identical spheres in a gravitational field. Because of its simplicity the coaxial three-sphere configuration affords a convenient comparison between theory and experiment in which the unsteady effects of the virtual mass and Basset forces can be carefully examined over a long time scale with large particle displacements. The theoretical and experimental results presented in this investigation are, to the authors' knowledge, the first carefully documented confirmation of the presence of the Basset force effect. These results show that for slowly changing multiparticle gravitational motions the Basset force is the most important inertial effect at low but non-zero Reynolds numbers.

The qualitative behaviour of the coaxial three-sphere problem with an initial configuration as

shown in figure 1 *a* was first investigated experimentally by Happel & Pfeffer (1960). They observed that if three spheres were released from rest, 1 and 2 would initially fall as a doublet at a velocity that Stokes theory predicts would be 55 % greater than the settling velocity of a similar isolated sphere of the same diameter. The flow configuration shown in figure 1 *a*, therefore, does not persist. As spheres 1 and 2 approach sphere 3, sphere 2 starts to accelerate due to its combined interaction with spheres 1 and 3, as shown in figure 1 *b*. Finally, as sphere 2 approaches sphere 3, 2 and 3 form a doublet which continues to move away from sphere 1, figure 1 *c*, as long as the spheres are allowed to settle without approaching or impinging on any boundaries. An intriguing new facet of the three-sphere interaction problem that was discovered during the course of the present investigation is the 'critical initial spacing' condition described in § 7. One finds that the gap between the two leading spheres of three-sphere and longer chains can asymptote with time either to zero or to some finite non-zero gap, depending on the initial configuration. A 'critical spacing' curve separates the sets of initial configurations which produce these two different asymptotic behaviours.

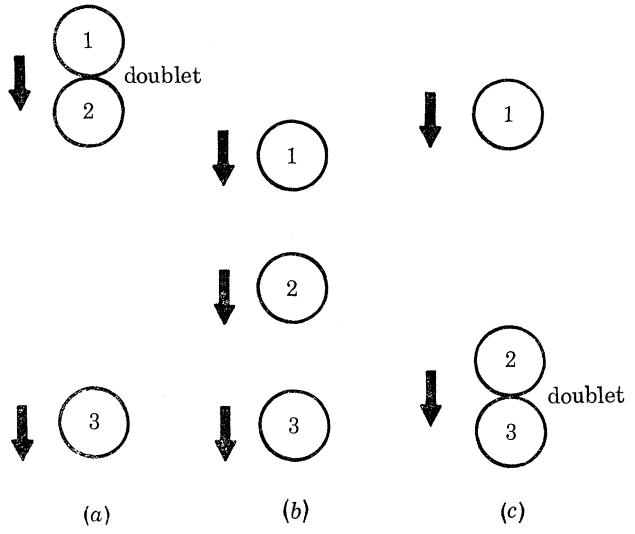

FIGURE 1. Gravity settling of three spheres.

In principal the quasi-steady state Stokes drag on a sphere in strong interaction can be determined by one of several approaches: the method of reflexions, finite element methods, or the boundary method used in this work. The method of reflexions, developed by Smoluchowski (1911) and used widely by others, is most satisfactory for weak interactions in which only a single reflexion from each boundary is required. The method converges very slowly for closely spaced objects and is laborious to apply when multiple reflexions from more than two solid bodies are considered. Several investigators have recently applied finite-element methods to multiparticle slow flows. For example, Skalak, Chen & Chien (1972) have used the method to model capillary blood flow. The red cells are simulated by bi-concave disk-shaped solid particles which are equally spaced and axisymmetrically located in a circular tube. This method is a very promising technique for studying irregular but identical particles with periodic spacing.

Of the three methods the one that offers the greatest flexibility, ease of application, and accuracy for treating closely spaced multiparticle flows is the discrete point boundary method developed by Gluckman, Pfeffer & Weinbaum (1971) and Gluckman, Weinbaum & Pfeffer

(1972). In the former paper it is shown that the disturbances due to each submerged sphere or spheroid in an arbitrary coaxial distribution of spheres or spheroids can be exactly represented by an infinite series of multilobular disturbances, or multipoles, located at the origin of each object. These disturbances are described by the simply separable singular solutions of the axisymmetric Stokes equation written in a local spherical or spheroidal coordinate system corresponding to the surface of each object. Solutions to any degree of accuracy can be obtained depending on the order of truncation or number of multipoles retained in the solution. Since the method is one of truncation rather than iteration, in which all particles are treated simultaneously for interactions of any order, the solution procedure converges extremely rapidly and provides good drag estimates even for the lowest-order truncation. For example, in the most extreme case of two spheres touching, the first, third and fifth order truncation solutions yield drag approximations which are within 2.5, 0.14 and 0.001 % of the exact solution, respectively. In Gluckman *et al.* (1972) this theory is extended to treat the axisymmetric flow past an arbitrary body of revolution

Section 2 briefly summarizes the dynamic equation of motion for a single sphere, while § 3 describes how each of the force components must be modified for a multiparticle system. The quasi-steady equations for axisymmetric creeping flow with particle interaction are presented in § 4. Section 5 describes the near collision behaviour of two spheres that approach each other with a finite relative velocity. The numerical solution of the nonlinear dynamic equations of motion is discussed in § 6. Sections 7 and 8 present the results for three-sphere and longer chains, respectively, which are settling coaxially under the effect of gravity.

2. Formulation of the dynamic equations of motion for a single sphere

The momentum equation for unsteady creeping motion is

$$\frac{\partial \boldsymbol{V}}{\partial t} = -\frac{1}{\rho}\nabla p + \nu\nabla^2 \boldsymbol{V}. \tag{2.1}$$

To eliminate the pressure one takes the curl of (2.1)

$$\frac{\partial(\operatorname{curl} \boldsymbol{V})}{\partial t} = \nu\nabla^2(\operatorname{curl} \boldsymbol{V}). \tag{2.2}$$

Landau & Lifshitz (1959) present an elegant analysis of equation (2.2) and solve it for the case of a single sphere moving slowly with velocity $U(t)$ in a viscous fluid. The solution is found by representing the velocity $U(t)$ as a Fourier integral,

$$U(t) = \int_{-\infty}^{\infty} U_\omega \, \mathrm{e}^{-\mathrm{i}\omega t} \, \mathrm{d}\omega,$$

where U_ω is the solution to (2.1) for a sphere oscillating with frequency ω. The expression for the drag force F on the sphere is given in terms of $U(t)$ as

$$F = 6\pi\mu U a + \tfrac{2}{3}\pi\rho a^3 \frac{\mathrm{d}U}{\mathrm{d}t} + 6\pi\mu a^2 \frac{1}{\sqrt{(\pi\nu)}} \int_0^t \frac{\mathrm{d}U}{\mathrm{d}\tau} \frac{\mathrm{d}\tau}{\sqrt{(t-\tau)}}. \tag{2.3}$$

Equation (2.3) shows that there are three basic contributions to the drag force on a sphere undergoing an arbitrary slow motion in a viscous fluid. The first force component in equation

(2.3) is the steady-state Stokes drag contribution. The remaining two terms represent unsteady contributions to the drag force – the virtual or hydrodynamic mass contribution and the Basset force (after Basset 1888; see Brenner 1961).

The complete equation of motion for the unsteady settling of a single sphere at low Re in an unbounded viscous fluid is obtained by adding the gravity and buoyancy forces to the three dynamic forces in (2.3) and equating the sum to the acceleration force of the sphere

$$\tfrac{4}{3}\pi a^3\rho_s\frac{\mathrm{d}U}{\mathrm{d}t} = \tfrac{4}{3}\pi a^3(\rho_s-\rho)\,g - 6\pi\mu Ua - \tfrac{2}{3}\pi a^3\rho\frac{\mathrm{d}U}{\mathrm{d}t} - 6\pi\mu a^2\frac{1}{\sqrt{(\pi\nu)}}\int_0^t\frac{\mathrm{d}U}{\mathrm{d}\tau}\frac{\mathrm{d}\tau}{\sqrt{(t-\tau)}}, \tag{2.4}$$

where a is the sphere radius, ρ_s the sphere density, ρ the fluid density, and μ is the fluid viscosity $= \nu\rho$.

The simple summation of forces (2.4) is strictly valid only in the limit as Re approaches zero where the governing equation (2.1) is linear. The terminal settling velocity U_t is found from (2.4) by settling $\mathrm{d}U/\mathrm{d}t = 0$,

$$U_t = \frac{2a^2(\rho_s-\rho)\,g}{9\mu}. \tag{2.5}$$

In order to determine the relative magnitude of each of the terms appearing in (2.4) all the variables will be made dimensionless by introducing characteristic reference quantities. Denoting dimensionless variables by a tilde,

$$\tilde{U} = U/U_t, \quad \tilde{t} = tU_t/a, \quad \tilde{\rho} = \rho_s/\rho, \tag{2.6}$$

and substituting in (2.4), one obtains

$$\mathrm{Re}_\infty(\tilde{\rho}+\tfrac{1}{2})\frac{\mathrm{d}\tilde{U}}{\mathrm{d}\tilde{t}} = 9(1-\tilde{U}) - \frac{9\,\mathrm{Re}_\infty^{\frac{1}{2}}}{\sqrt{(2\pi)}}\int_0^{\tilde{t}}\frac{\mathrm{d}\tilde{U}}{\mathrm{d}\tilde{\tau}}\frac{\mathrm{d}\tilde{\tau}}{\sqrt{(\tilde{t}-\tilde{\tau})}}, \tag{2.7}$$

where

$$\mathrm{Re}_\infty = \frac{2aU_t}{\nu} = \frac{2a^2}{\nu}\Big/\frac{a}{U_t} \tag{2.8}$$

is the Reynolds number based on the sphere's diameter and terminal settling velocity.

The Reynolds number defined in (2.8) represents the ratio of two characteristic reference times, a molecular diffusion time a^2/ν, and a macroscopic time a/U_t characterizing the hydrodynamic–gravitational interaction. One therefore suspects that when $\mathrm{Re}_\infty \ll 1$ there are two time scales in the problem of spheres which start falling from rest. On the longer time scale $\tilde{t}$ defined in (2.6), whose dimensional characteristic time is a/U_t, the unsteady terms in (2.7) are higher order in Re_∞. If the solution for $\tilde{U}$ is written as an expansion in half-powers of the Reynolds number

$$\tilde{U} = \sum_{n=0}\mathrm{Re}_\infty^{\frac{1}{2}n}\,\tilde{U}_n, \tag{2.9}$$

one can readily show that the solution to equation (2.7) for large times is

$$\tilde{U}_0 = 1, \quad \tilde{U}_1 = \tilde{U}_2 = \ldots = 0. \tag{2.10}$$

An isolated sphere thus achieves a constant settling velocity since in the absence of other boundaries the flow geometry is constant. In contrast, the solution for $\tilde{U}_0$ is not constant even for large times if three or more spheres are present since hydrodynamic interactions slowly change the sphere spacing and settling velocity as the motion progresses. The interesting observation whose implications have not been studied before is that on the long time scale over which these

hydrodynamic interactions occur, the Basset force term which is $O(\mathrm{Re}_\infty^{\frac{1}{2}})$ dominates over both the inertial and virtual-mass terms which are $O(\mathrm{Re}_\infty)$ in equation (2.7). One can also show that on this long time scale, the convective $\boldsymbol{V}\cdot\nabla\boldsymbol{V}$ term in the Navier–Stokes equation is $O(\mathrm{Re}_\infty)$ by comparison with the viscous and pressure terms, and thus may also be neglected in comparison with the Basset force to $O(\mathrm{Re}_\infty^{\frac{1}{2}})$. The coaxial settling of three spheres thus provides a simple convenient experiment in which the presence of the Basset force can be experimentally verified and theoretically examined over a long time scale.

It is evident that (2.10) cannot satisfy the initial condition, $\tilde{U} = 0$, and that a shorter time scale must exist, representing the initial period of rapid acceleration $\mathrm{d}\tilde{U}/\mathrm{d}\tilde{t} \gg O(1)$, during which the spheres attain their quasi-steady settling velocity. Inspection of (2.7) suggests that during the initial period we redefine dimensionless time by

$$t^* = \mathrm{Re}_\infty^{-1}\tilde{t}.$$

Substituting in (2.7), one obtains

$$(\tilde{\rho}+\tfrac{1}{2})\frac{\mathrm{d}\tilde{U}}{\mathrm{d}t^*} = 9(1-\tilde{U}) - \frac{9}{\sqrt{(2\pi)}}\int_0^{t^*}\frac{\mathrm{d}\tilde{U}}{\mathrm{d}t^*}\frac{\mathrm{d}t^*}{\sqrt{(t^*-\tau^*)}}. \tag{2.11}$$

One observes that all terms in (2.11) are $O(1)$ and must be retained during the initial period in which $\mathrm{d}\tilde{U}/\mathrm{d}t^* = O(1)$ and $\tilde{t}$ is of $O(\mathrm{Re}_\infty)$. On the other hand, the nonlinear $\boldsymbol{V}\cdot\nabla\boldsymbol{V}$ term in the Navier–Stokes equation is $O(\mathrm{Re})$ smaller than the viscous and unsteady inertia terms on this shorter time scale. It is therefore consistent to neglect convective inertial effects while retaining the unsteady inertial, virtual-mass and Basset forces in (2.11). Experimentally, the importance of the Basset force is difficult to isolate on this time scale since the initial transient phase is short-lived and the other unsteady forces are of the same order.

3. Correction of the dynamic forces

In order to apply (2.4) to a low Re flow system with three or more spheres, each of the dynamic force contributions must be modified to take into account particle interaction effects. Each dynamic force correction will be considered separately in the next three subsections.

(*a*) *Stokes drag force*, $F_{\mathrm{d.}}$

The viscous drag term used in the dynamic equations (2.4) and (2.7) is the well-documented Stokes drag force on a single sphere settling in an unbounded viscous fluid for $\mathrm{Re} \ll 1$, $F_{\mathrm{d.}} = 6\pi\mu a U$. When more than one sphere is present in the system, this expression for the drag force can be simply modified to account for particle interaction effects on each sphere by introducing an interaction parameter λ_j which is a function of all the sphere spacings and velocities and is defined for sphere j by

$$F_{\mathrm{d.},j} = 6\pi\mu U_j a\lambda_j. \tag{3.1}$$

The multipole truncation technique, developed in Gluckman *et al.* (1971) for multiple equally spaced coaxial spheres and spheroids is ideally suited for the computation of λ_j.

The geometry being considered is shown in figure 2 for N spheres. The exact solution for the stream function from Gluckman *et al.* (1971) is given by the superposition of N infinite series representing the disturbance produced by each of the N spheres.

$$\psi = \sum_{j=1}^{N}\sum_{n=2}^{\infty}[B_{nj}r_j^{-n+1} + D_{nj}r_j^{-n+3}]\mathscr{T}_n(\zeta_j), \tag{3.2}$$

where $\mathscr{T}_n(\zeta)$ are Gegenbauer functions of the first kind,

$$r = [(z-z_j)^2+R^2]^{\frac{1}{2}}, \quad \zeta_j = \cos\theta_j = (z-z_j)/r_j,$$

z_j is the z coordinate of centre of sphere j, and $B_{nj}D_{nj}$ are constants.

Each term in the inner summation, termed a multipole, is a fundamental singular solution of the steady creeping motion equation obtained by dropping the unsteady term in equation (2.1) or (2.2). Each fundamental solution contains an amplitude function shown in brackets and a multilobular Gegenbauer function $\mathscr{T}_n(\zeta_j)$. The B_{nj} and D_{nj} coefficients which fix the strength of the multipole are determined by satisfying the no slip boundary conditions over the generating arcs of all spheres simultaneously, i.e.

$$V_z = \frac{1}{R}\frac{\partial\psi}{\partial R} = U_j, \qquad V_R = -\frac{1}{R}\frac{\partial\psi}{\partial z} = 0. \qquad \text{on } r_j = a;\ j = 1, \ldots, N \tag{3.3}$$

To satisfy the boundary conditions (3.3) exactly along the entire surface of each sphere would require the solution of an infinite array of unknown coefficients. However, solutions to any desired accuracy can be obtained by a uniform truncation of each of the infinite multipole series.

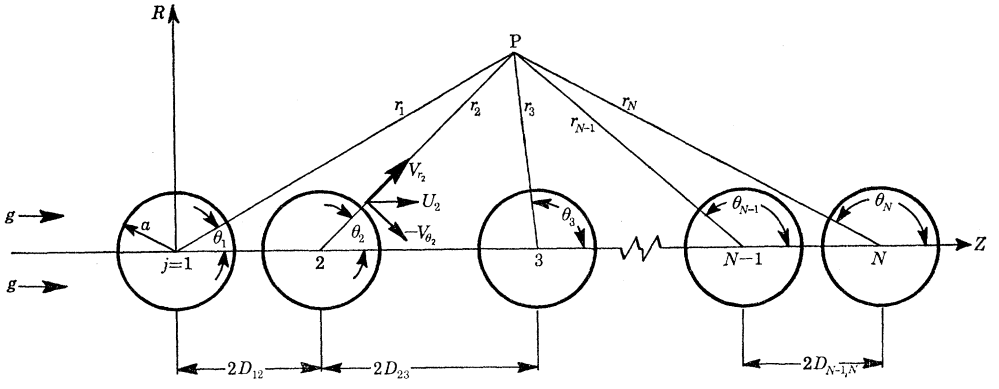

FIGURE 2. Geometry of N-sphere system.

The two unknown coefficients in each multipole permit one to satisfy the exact no slip boundary conditions (3.3) at one discrete point on the generating arc of each sphere. Thus, if a spherical boundary is to be approximated by satisfying conditions (3.3) at M discrete points on its generating arc, M terms are retained in the multipole expansion for each sphere. In general, one obtains a set of $2\times M\times N$ simultaneous linear algebraic equations for the $2\times M\times N$ unknown B_{nj} and D_{nj} coefficients. The desired matrix solution for these coefficients, the procedure for choosing boundary points and the convergence properties of the solution are described in detail in Gluckman *et al.* (1971).

One can show that the Stokes drag correction factor λ_j in (3.1) depends only on the D_{nj} coefficients in the series solution (3.2). This result is

$$\lambda_j = D_{2j}/1.5U_j a. \tag{3.4}$$

The λ_j are only functions of the distances between spheres and their relative velocities.

An examination of the λ_j for three spheres moving at the same velocity for various sphere spacings provides the basic physical insight into the qualitative experimental observations of

Happel & Pfeffer (1960) shown in figure 1. This is shown in figure 3 where we have plotted curves of λ_j against a spacing parameter $b/(b+c)$ for two values of the overall spacing $(b+c)$. One observes that the drag on the centre sphere is always less than the drag on either of the outer spheres. This is due to the fact that, unlike the outer spheres, the central sphere is being acted on directly by both neighbours. This suggests that, whatever the starting position of the three spheres, the central sphere will attempt to approach sphere 3. Therefore, one should always move to the right along the $b/(b+c)$ axis as time progresses. Finally, it is of interest to note that as spheres 2 and 3 move away from the single sphere 1, λ_1 will approach unity, whereas λ_2 and λ_3 will approach a constant value which depends on the asymptotic spacing c_∞ after sphere 1 has been left far behind.

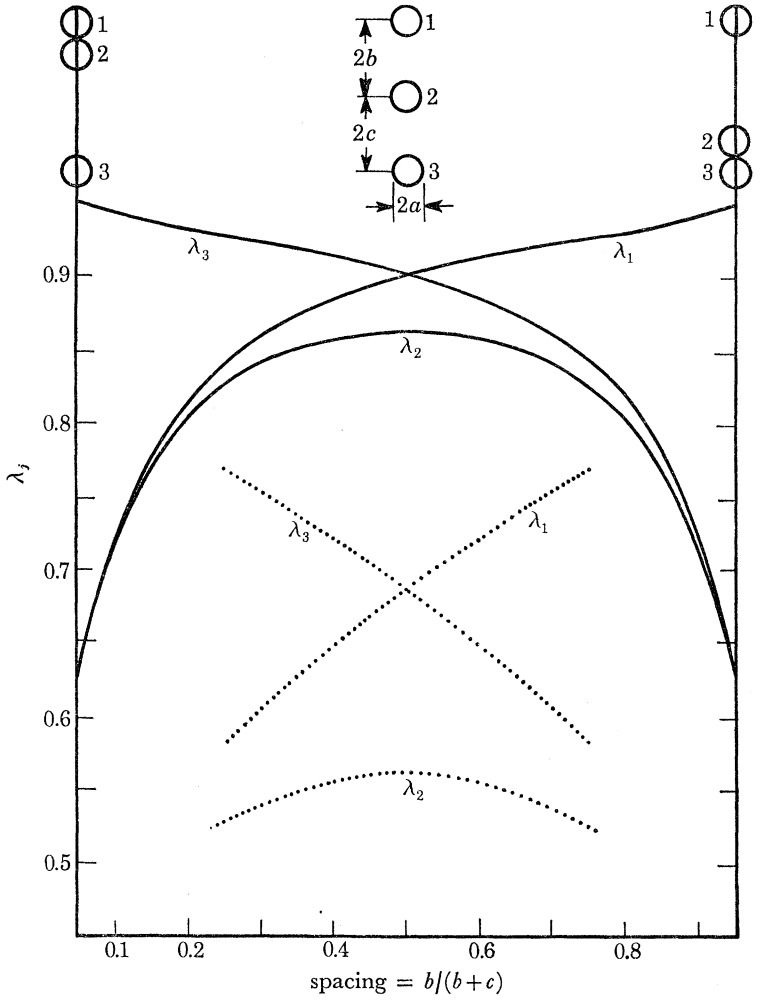

FIGURE 3. λ_j plotted against spacing for three spheres.
——, $b+c = 20a$; ..., $b+c = 4a$.

(b) *Virtual mass term, $F_{\text{v.m.}}$*

Virtual mass has been defined by Darwin (1953) as the mass of fluid to be added to that of the solid in calculating its kinetic energy. Existing calculations of this additional apparent mass, as well as its derivation, have been based on arguments derived from ideal fluid theory. For viscous flow both the rotational and irrotational solutions in equation (3.2) contribute to the kinetic

energy of the fluid. The potential flow component of the solution differs from ideal fluid theory in that the normal velocity component due to just the irrotational terms in (3.2) does not vanish at the sphere surface. Landau & Lifshitz (1959), however, show that for the case of a single sphere moving with an arbitrary velocity $\boldsymbol{u}(t)$ in a real fluid at zero Re_∞ the virtual mass due to the sum of the irrotational and rotational contributions is identical to that for the given sphere moving in a potential flow with the same velocity. We shall assume that this result is also valid for more than one sphere although a rigorous justification is theoretically difficult and not warranted for the present application. Our purpose here is simply to obtain an estimate of the importance of the other spheres in calculating the virtual mass contribution for any given sphere.

In general, the virtual mass (v.m.) of an object is given by

$$\text{virtual mass} = kM', \tag{3.5}$$

where M' is the mass of the fluid displaced by the object and k is a configuration parameter depending on the object shape and the interaction effects that arise from the presence of other boundaries. For a single sphere in an infinite medium, $k = 0.5$.

One can show by using Green's theorem (see, for example, Milne-Thomson 1960, p. 89) that when the motion is irrotational the kinetic energy of the fluid can be represented by

$$T = -(\tfrac{1}{2}\rho)\oint \phi \frac{\partial \phi}{\partial n}\,\mathrm{d}A = -\pi\rho \oint \frac{\psi_\mathrm{p}}{r\sin\theta}\frac{\partial \psi_\mathrm{p}}{\partial n}\,\mathrm{d}s, \tag{3.6}$$

where ϕ is the velocity potential, $\mathrm{d}n$ is an element of normal drawn into the fluid at the element $\mathrm{d}A$ of surface, ψ_p is the stream function in potential flow and $\mathrm{d}s$ the element of integration path along the generating arc of a body of revolution, and the integral is performed in a clockwise sense about all boundaries. The contribution to the kinetic energy integral (3.6) from each sphere is

$$T_j = \pi\rho \int_0^\pi \frac{a\psi_\mathrm{p}}{r_j \sin\theta_j}\frac{\partial \psi_\mathrm{p}}{\partial r_j}\,\mathrm{d}\theta_j. \tag{3.7}$$

To find the value of k for sphere j, which we denote as k_j, we equate the time rate of change of T_j to the work done by an external force applied to sphere j to provide its acceleration. The resulting expression for k_j is

$$k_j = \frac{1}{\frac{4}{3}\pi a^3 \rho}\left(\frac{2T_j}{U_j^2}\right). \tag{3.8}$$

The series solution to the axisymmetric potential flow equation for the potential flow stream function ψ_p is simply the irrotational portion of the series solution (3.2). For a system of three spheres

$$\psi_\mathrm{p} = \sum_{j=1}^{3}\sum_{n=2}^{\infty} B_{nj} r_j^{-n+1}\mathscr{T}_n(\cos\theta_j). \tag{3.9}$$

The B_{nj} constants in (3.9) can be evaluated by requiring that the normal velocity component vanish at discrete points on the surface of each sphere. The method is entirely analogous to the solution of equation (3.2) for viscous flow described in the previous subsection.

The values of T_j in equation (3.7) have been calculated for various sphere configurations using a five-term truncation to the series solution (3.9) and the configuration parameters k_j evaluated from equation (3.8). The values of k_3 determined by the above procedure have been plotted in figure 4 for the range $1 \leqslant b \leqslant 8$, $1 \leqslant c \leqslant 8$, where b and c are defined in the figure, assuming

that all three spheres have the same velocity. This figure indicates that the maximum deviation from a single sphere value $k = \frac{1}{2}$ occurs, as would be expected, when the three spheres are touching. As the distance between spheres 3 and 2 increases, k_3 rapidly asymptotes to the single sphere value of $\frac{1}{2}$. The greatest deviation exhibited by k_3 from the value of $\frac{1}{2}$ is approximately 10 %. This deviation occurs only when spheres 2 and 3 are touching and drops off rapidly to approximately 2 % when these spheres are two diameters apart. This exercise demonstrates that in a three sphere system and, presumably, in systems of more than three spheres, particle interaction effects influence the virtual mass associated with each sphere to a relatively minor extent, even when the spheres are close together. Since the virtual mass forces are higher order in Re_∞ than

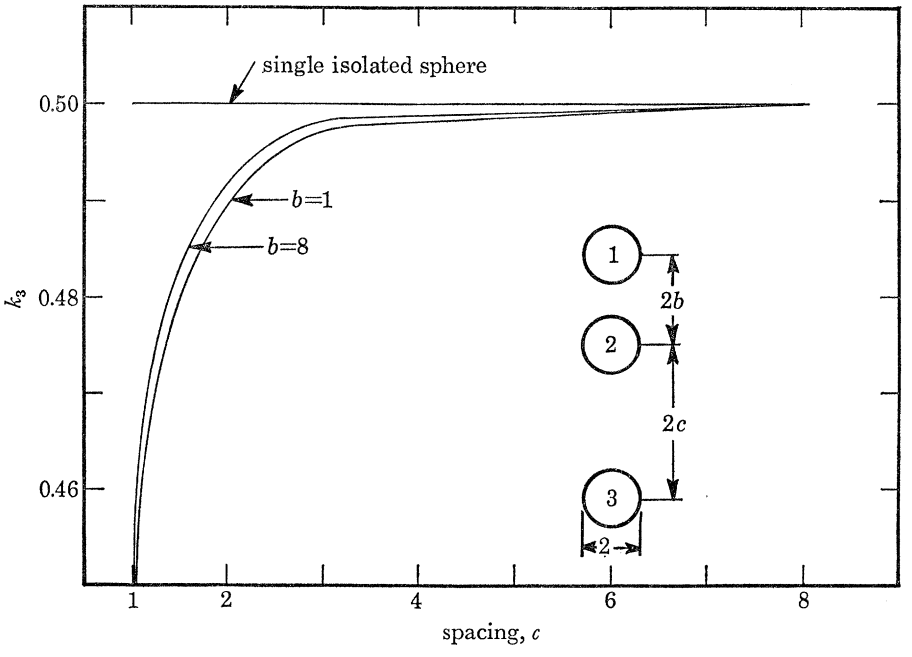

FIGURE 4. Deviation in virtual mass parameter k_3 versus system geometry.

the Basset force contribution on the long time scale characterizing the important particle interaction effects and are significant only for the short initial period of large accelerations, the values of k_j used were considered to be constant and equal to $\frac{1}{2}$. By similar arguments, the assumption of using the potential flow value of $\frac{1}{2}$ for Stokes flow is reasonable, although this assumption has not been rigorously justified for the viscous motion of multi-body systems. The errors introduced by these assumptions should be small, while the assumptions themselves allow computing times to be reduced substantially.

(*c*) *Basset force*, F_{B}

The Basset force exerted on a sphere moving with an arbitrary velocity $U(t)$ can be constructed as a superposition integral in which the unit velocity impulsive motion of the sphere is treated as the basic solution. In the basic solution each segment of the solid boundary is treated locally as a Rayleigh problem for the impulsive motion of a flat plate. Unless the boundary continues to accelerate and generate vorticity the Basset force will decay as $1/\sqrt{t}$ during the initial period of acceleration, the total amount of vorticity being conserved but redistributed throughout the flow field. A precise treatment of this force for a multiparticle problem would require that this

basic unit solution take into account the instantaneous boundaries of the other spheres. Since the Basset force is a higher order correction of $O(\mathrm{Re}_\infty^{\frac{1}{2}})$ on the long time scale of significant interactions, and convective inertia terms of $O(\mathrm{Re})$ have already been neglected in the Navier–Stokes equation, it would seem reasonable to use as a lowest order approximation the unit solution for a single sphere. The close agreement between theory and experiment presented in § 7 lends further support to this approximation.

The neglect of the boundaries of the other spheres in the unit solution for the Basset force on the short initial time scale of large accelerations can be argued on similar grounds. From arguments of § 2, this time scale is of $O(\mathrm{Re}_\infty)$. Thus if the inner small time and outer large time solutions are to be valid to the same order in a matched asymptotic sense the use of the unit solution for a single sphere on the short time scale will introduce errors which are higher order than those already included in the model for the long time behaviour. Thus, we shall approximate $F_{\mathrm{B},j}$ on both time scales by its expression for a single sphere given in (2.4).

$$F_{\mathrm{B},j} = 6\pi\mu a^2 \frac{1}{\sqrt{(\pi\nu)}} \int_0^t \frac{\mathrm{d}U_j}{\mathrm{d}\tau} \frac{\mathrm{d}\tau}{\sqrt{(t-\tau)}}. \tag{3.10}$$

It should be noted, however, that although this approximation is valid for motion in an unbounded medium, the effect of an enclosing boundary on the Basset force may be significant, particularly for particles in close proximity to the wall. Transient motions in bounded media should, therefore, be handled more carefully.

4. Equations of motion for three or more spheres

Based on the discussions presented in §§ 2 and 3, the equation of motion for any sphere j in an N-sphere chain can be represented, using equations (2.7) and (3.1), by

$$\mathrm{Re}_\infty(\tilde{\rho}+\tfrac{1}{2}) \frac{\mathrm{d}\tilde{U}_j}{\mathrm{d}\tilde{t}} = 9(1-\tilde{U}_j\lambda_j) - \frac{9\,\mathrm{Re}_\infty^{\frac{1}{2}}}{\sqrt{(2\pi)}} \int_0^{\tilde{t}} \frac{\mathrm{d}\tilde{U}_j}{\mathrm{d}\tilde{\tau}} \frac{\mathrm{d}\tilde{\tau}}{\sqrt{(\tilde{t}-\tilde{\tau})}} \quad (j = 1, 2, \ldots, N). \tag{4.1}$$

The position of each sphere is obtained by integrating

$$\frac{\mathrm{d}\tilde{x}_j}{\mathrm{d}\tilde{t}} = \tilde{U}_j \quad (j = 1, 2, \ldots, N), \tag{4.2}$$

where $\tilde{x}_j$ is a dimensionless length x_j/a, subject to initial conditions based on the initial sphere spacing.

In accord with our previous analysis, sphere interaction effects in the N equations (4.1) are described by the λ_j factors applied to each Stokes drag term, whereas both the virtual mass and Basset forces are approximated by their single sphere expressions. This approximation should be valid to $O(\mathrm{Re}_\infty^{\frac{1}{2}})$ on both the short and long time scales.

In the limit $\mathrm{Re}_\infty = 0$, equations (4.1) and (4.2) reduce to

$$\tilde{U}_j\lambda_j = 1 \quad (j = 1, 2, \ldots, N) \tag{4.3}$$

$$\frac{\mathrm{d}\tilde{x}_j}{\mathrm{d}\tilde{t}} = \frac{1}{\lambda_j}. \tag{4.4}$$

Equation (4.3) which replaces the single-sphere equation (2.10) describes the behaviour on the long time scale to lowest order for small but finite Re_∞. To this order, particle interaction effects contained in λ_j are undergoing changes of order unity.

PHILOSOPHICAL TRANSACTIONS OF THE ROYAL SOCIETY A MATHEMATICAL, PHYSICAL & ENGINEERING SCIENCES

The equations of motion, equations (4.1) and (4.2) or equations (4.3) and (4.4), were integrated numerically. Before describing the integration procedure and the results, we shall digress briefly to consider the separate problem of two spheres undergoing a 'near' collision in Stokes flow.

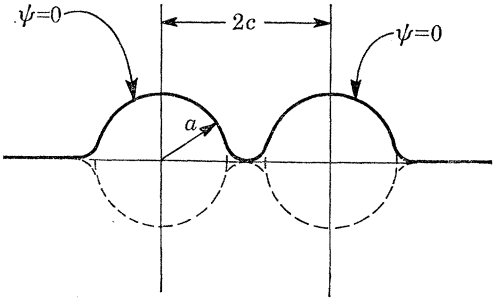

FIGURE 5. Deviation in the $\psi = 0$ streamline predicted by truncation technique.

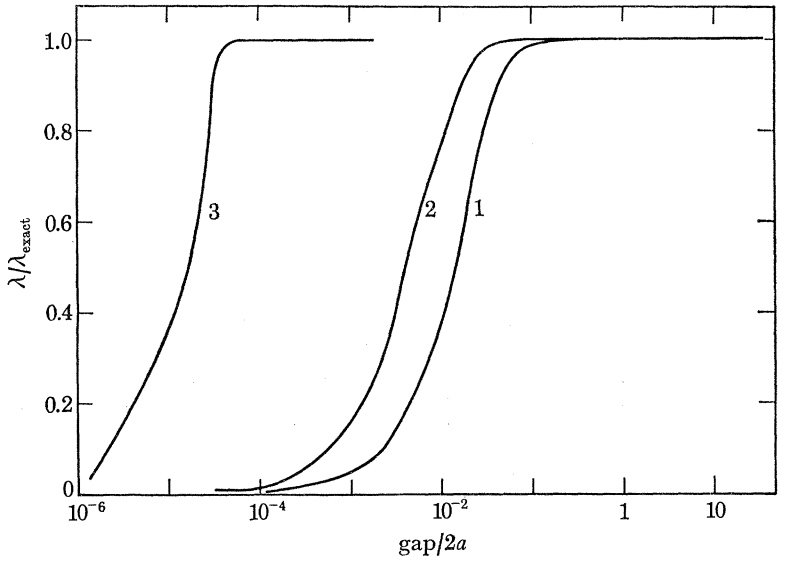

FIGURE 6. Comparison of predicted and exact drags: (1) 9 points, (2) 21 points, (3) 5 points starting at one degree.

5. ON THE NEAR-COLLISION APPROACH OF TWO SPHERES

Due to the nature of the interparticle interactions in chains of three or more spheres, the gap separating the leading doublet of such chains must monotonically decrease with time. The numerical results of the present work indicate that if the initial configuration falls below the 'critical spacing' curve in figure 7 the gap eventually tends to zero as the two spheres head toward an apparent collision.

The equations of motion (4.1) and (4.2) do not permit this impact, since an infinite force is theoretically required to remove the last element of fluid trapped in the narrowing gap. Indeed, it is well known that the resistance to the approach of two surfaces is inversely proportional to the gap between them. Since the forces in the problem are bounded, it follows that the gap will tend to zero asymptotically, and that actual contact will not be made in any finite time.

The problem of two spheres approaching each other is identical to the problem of a single sphere falling toward a planar free surface. The exact solution for this problem has been developed by Brenner (1961):

$$\lambda = \tfrac{4}{3}\sinh\alpha \sum_{n=1}^{\infty} \frac{n(n+1)}{(2n-1)(2n+3)} \left[\frac{4\cosh^2(n+\tfrac{1}{2})\alpha + (2n+1)^2\sinh^2\alpha}{2\sinh(2n+1)\alpha - (2n+1)\sinh 2\alpha} - 1\right], \tag{5.1}$$

where $\alpha = \operatorname{arcosh}(\tilde{c})$, $\tilde{c} = c/a$, $2c$ is the centre-to-centre spacing between the spheres. It is seen from (5.1) that as $\tilde{c} \to 1$ the drag force goes to infinity, as expected.

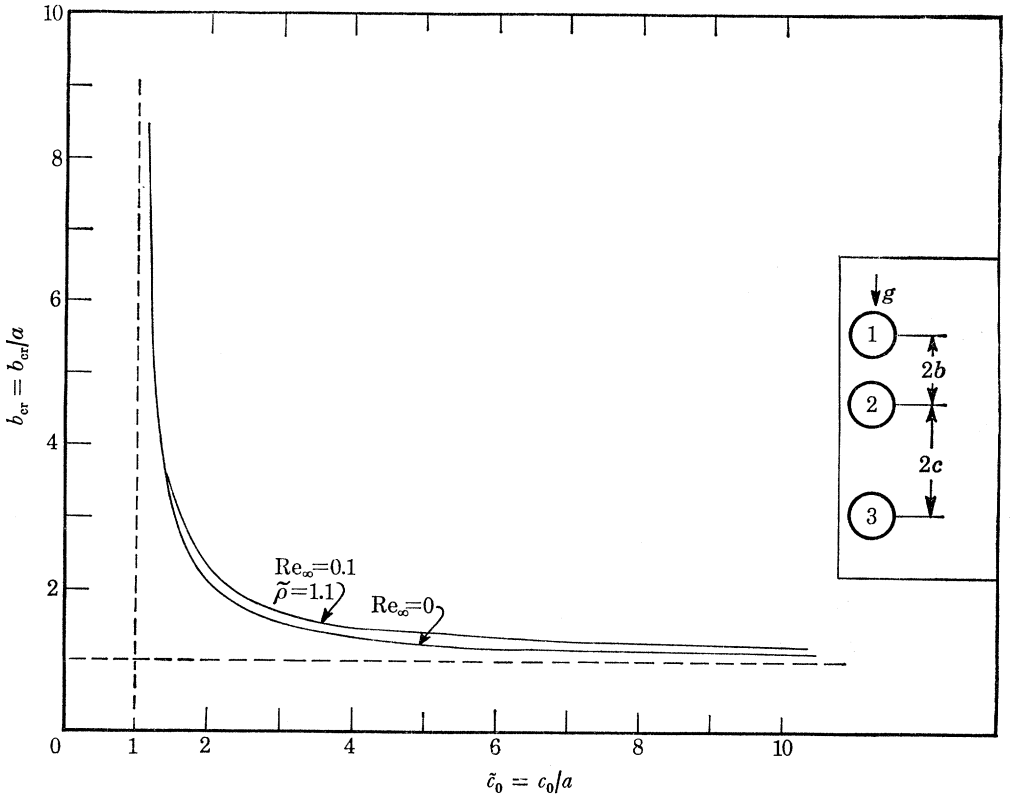

FIGURE 7. Critical initial spacing curves for $\mathrm{Re}_\infty = 0$ and 0.1.

The multipole truncation technique developed in Gluckman *et al.* (1971) requires special refinement as $\tilde{c} \to 1$. The difficulty stems from the fact that the coefficient matrix for the B_{nj} and D_{nj} coefficients is singular when the front and rear stagnation points are included in the set of boundary-condition points. Exclusion of these points from the set results in a zero streamline whose shape, shown in figure 5, deviates from sphericity near the axis, where two small cusps appear.

It is evident from figure 5 that as $\tilde{c} \to 1$, special treatment must be given to the selection of boundary points near the axis. The special procedure that has been developed for near collision flow is illustrated in figure 6 where we have plotted the ratio of the multipole truncation technique drag results to the exact drag (5.1) against the dimensionless gap, $\tilde{c} - 1$, for two approaching spheres. In curve 1, boundary conditions are satisfied at nine points equally spaced on the generating arc, starting at $\theta = 18°$. Twenty-one points are used for curve 2, similarly distributed, starting at $\theta = 8.2°$. Curve 3 is for five points, with the lowest at one degree above the centreline.

One concludes from figure 6 that the agreement with (5.1) is excellent for large spacings, but breaks down as the gap narrows to about 0.1, 0.03 and 0.0005 diameters for the three respective cases. All three curves asymptote to zero as the gap vanishes and as the exact drag force becomes infinite. The marked improvement exhibited by curve 3 over curves 1 and 2 is attributed to the closer proximity of the lowest boundary-condition point to the centreline, reducing the size of the cusp and allowing a closer approach before the solution breaks down. Reducing the angle further below 1° is not rewarded with additional accuracy, since the matrix equation becomes ill-conditioned, approaching a singular state as the angle vanishes.

In accordance with the above discussion, the particle velocities calculated in the time-dependent solution are accurate up to a point in time just prior to the erroneously predicted collision. At that point it will be understood that the relative velocity between the two spheres drops rapidly toward zero and that contact can only be made after an infinite time. A similar transient behaviour was reported by Wacholder & Sather (1974).

6. Numerical integration procedure

The time dependent velocities and trajectories of the N spheres of a given chain were calculated numerically by integrating the equations of motion, equations (4.1) and (4.2) for $0 < \mathrm{Re}_\infty \ll 1$, or (4.3) and (4.4) for $\mathrm{Re}_\infty = 0$. In either case, the system of $2N$ equations for $\tilde{U}_1, \tilde{U}_2, \ldots, \tilde{U}_N$, $\tilde{x}_1, \tilde{x}_2, \ldots, \tilde{x}_N$ is highly nonlinear, since each of the drag correction factors, λ_j, is itself a function of these dependent variables, all of which enter into the matrix equation.

This matrix equation is created by the simultaneous application of no-slip boundary conditions at all points. The boundary conditions (3.3) obtained by differentiating the general solution (3.2), when applied at any point m on the generating arc of the jth sphere, can be represented as follows:

$$\left.\begin{aligned} v_z &= \sum_{q=1}^{N}\sum_{n=2}^{M+1}[B'_{nqm}B_{nq}+D'_{nqm}D_{nq}] = U_j, \\ v_R &= \sum_{q=1}^{N}\sum_{n=2}^{M+1}[B''_{nqm}B_{nq}+D''_{nqm}D_{nq}] = 0, \end{aligned}\right\} \quad (1 \leqslant m \leqslant M, \quad j = 1, \ldots, N) \tag{6.1, 6.2}$$

where

$$\left.\begin{aligned} B'_{nqm} &= r_{qm}^{-n-1}P_n(\zeta_{qm}), \\ D'_{nqm} &= r_{qm}^{1-n}[P_n(\zeta_{qm}) + 2\mathscr{T}_n(\zeta_{qm})], \\ B''_{nqm} &= r_{qm}^{-n-1}\left[\frac{(n+1)\,\mathscr{T}_{n+1}(\zeta_{qm})}{\sin\theta_{qm}}\right], \\ D''_{nqm} &= r_{qm}^{1-n}\left[\frac{(n+1)\,\mathscr{T}_{n+1}(\zeta_{qm}) - 2\zeta_{qm}\mathscr{T}_n(\zeta_{qm})}{\sin\theta_{qm}}\right]. \end{aligned}\right\} \tag{6.3}$$

When repeated for all values of m and j, these equations form a system of $2 \times M \times N$ equations for an equal number of unknown B_{nq} and D_{nq} coefficients, as discussed in § 3 (*a*).

For the sake of clarity, the integration procedure for the simpler equations (4.3) and (4.4) will be presented first. The sphere velocities at a given time can be calculated from equations (4.3) for any given set of sphere positions or spacings as follows. Combining (4.3) with (3.4) yields

$$D_{2j} = 1.5a \quad (j = 1, 2, \ldots, N). \tag{6.4}$$

That is, the sphere velocities are such that the viscous drag forces acting on the spheres are all constant with time, and are equal to the buoyancy force, as expected in the absence of acceleration-related effects. If D_{2j} is replaced by (6.4) N times in each of the $2 \times M \times N$ equations of

(6.1) and (6.2), and if the N sphere velocities, U_j, are treated as unknowns, then a simple transposition of terms in (6.1) and (6.2) will result in a new set of linear simultaneous algebraic equations for $2 \times M \times N$ unknowns ($B_{2j}, U_j, B_{nj}, D_{nj}$, where $n = 3, 4, \ldots, M+1$ and $j = 1, 2, \ldots, N$), which is solvable by matrix reduction. Thus, the velocities which satisfy (4.3) can be calculated directly, given the configuration, $\tilde{x}_1, \tilde{x}_2, \ldots, \tilde{x}_N$ (which must be known for the evaluation of (6.3)).

The initial conditions are set on the sphere spacings, while the initial velocities are calculated as those which satisfy (4.3) at the specified initial configuration. The system cannot be prescribed as starting from rest with $\mathrm{Re}_\infty = 0$, since equation (4.3) is incapable of describing the short initial acceleration period.

To integrate (4.3)–(4.4), discretize time and consider the kth time step, $\tilde{t}_{k-1} \leqslant \tilde{t} \leqslant \tilde{t}_k$, where $\tilde{t}_k = \tilde{t}_{k-1} + \Delta\tilde{t}_k$, $k \geqslant 1$, $\tilde{t}_0 = 0$, and $\Delta\tilde{t}_k$ is generally varying with k. The acceleration is assumed constant over the interval

$$\left(\frac{\mathrm{d}\tilde{U}_j}{\mathrm{d}\tilde{t}}\right)_k = \frac{\tilde{U}_{j,k} - \tilde{U}_{j,k-1}}{\Delta\tilde{t}_k} \quad (j = 1, 2, \ldots, N;\ \tilde{t}_{k-1} \leqslant \tilde{t} \leqslant \tilde{t}_k). \tag{6.5}$$

Reasonable initial guesses for the $\tilde{U}_{j,k}$ ($j = 1, 2, \ldots, N$), the sphere velocities at $\tilde{t} = \tilde{t}_k$, are

$$\tilde{U}_{j,k} = \tilde{U}_{j,k-1} + \left(\frac{\mathrm{d}\tilde{U}_j}{\mathrm{d}\tilde{t}}\right)_{k-1} \Delta\tilde{t}_k \quad (j = 1, 2, \ldots, N). \tag{6.6}$$

These velocities are used to integrate (4.4),

$$\tilde{x}_{j,k} = \tilde{x}_{j,k-1} + \tfrac{1}{2}(\tilde{U}_{j,k} + \tilde{U}_{j,k-1})\Delta\tilde{t}_k \quad (j = 1, 2, \ldots, N). \tag{6.7}$$

The original guesses for $\tilde{U}_{j,k}$ can now be improved by solving for the velocities from the matrix equation (6.1) and (6.2) as outlined above, using the latest values of $\tilde{x}_{j,k}$ from (6.7) as parameters. This process is then repeated in an iterative loop with alternate improvements on $\tilde{x}_{j,k}$ and $\tilde{U}_{j,k}$ ($j = 1, 2, \ldots, N$) by (6.7) and by (6.4) and (6.1), (6.2), respectively, until satisfactory convergence is obtained.

The greatest error present in the above procedure is the one associated with the linearization of the $\tilde{U}_j(\tilde{t})$ curves over the Δt_k interval in (6.7). A Taylor series expansion of $\tilde{U}_{j,k}$ and $\tilde{x}_{j,k}$ about $\tilde{t} = \tilde{t}_k$ shows this error to be

$$-\tfrac{1}{12}(\Delta\tilde{t}_k)^3 \left(\frac{\mathrm{d}^2\tilde{U}_j}{\mathrm{d}\tilde{t}^2}\right)_{k-1}.$$

The error's magnitude can thus be estimated following convergence of the iteration procedure. If it is found that the percentage error exceeds ϵ, a pre-set error limit, the time interval $\Delta\tilde{t}_k$ is halved and the computations repeated. If, on the other hand, the error is less than 0.1ϵ, $\Delta\tilde{t}$ is doubled ($\Delta\tilde{t}_{k+1} = 2\Delta\tilde{t}_k$) before proceeding with the computation. In this manner, the time interval is variable, being continually optimized in order to minimize the computing time while maintaining a desired accuracy.

The integration of the more complicated equations (4.1) and (4.2) for $0 < \mathrm{Re}_\infty \ll 1$ follows similar lines. Initial conditions are prescribed on the particle trajectories (initial configuration) as well as on the velocities ($\tilde{U}_{j,0} = 0, j = 1, 2, \ldots, N$).

Considering the kth time step, one approximates $(\mathrm{d}\tilde{U}_j/\mathrm{d}\tilde{t})_k$ by (6.5) and writes (4.1) in a finite difference form,

$$\tilde{U}_{j,k} = \frac{1 - \alpha_{j,k} + \beta_{j,k}}{\lambda_{j,k} + \gamma_k}, \tag{6.8}$$

or
$$\lambda_{j,k} = \frac{1-\alpha_{j,k}+\beta_{j,k}}{\tilde{U}_{j,k}} - \gamma_k, \tag{6.9}$$

where
$$\alpha_{j,k} = \left(\frac{2\,\mathrm{Re}_\infty}{\pi}\right)^{\frac{1}{2}} \sum_{i=1}^{k-1} \left(\frac{\mathrm{d}\tilde{U}_j}{\mathrm{d}\tilde{t}}\right)_i [(\tilde{t}_k - \tilde{t}_{i-1})^{\frac{1}{2}} - (\tilde{t}_k - \tilde{t}_i)^{\frac{1}{2}}],$$
$$\beta_{j,k} = \gamma_k \tilde{U}_{j,k-1},$$
$$\gamma_k = \frac{\frac{1}{9}\,\mathrm{Re}_\infty(\tilde{\rho}+\frac{1}{2}) + ((2/\pi)\,\mathrm{Re}_\infty \Delta\tilde{t}_k)^{\frac{1}{2}}}{\Delta\tilde{t}_k}.$$

When combined with (3.4), equation (6.9) becomes
$$D_{2j} = 1.5a(1-\alpha_{j,k}+\beta_{j,k}) - 1.5a\gamma_k \tilde{U}_{j,k} \quad (j = 1, 2, \ldots, N). \tag{6.10}$$

The relation (6.10) is utilized in the same manner as (6.4) to transform (6.1) and (6.2) into a new matrix equation for the $2 \times M \times N$ unknowns B_{2j}, $\tilde{U}_j$, B_{nj}, D_{nj} ($n = 3, 4, \ldots, M+1$ and $j = 1, 2, \ldots, N$). Thus, once more, the set of velocities which satisfies (4.1) can be calculated directly for any given configuration, $\tilde{x}_1, \tilde{x}_2, \ldots, \tilde{x}_N$.

The rest of the procedure is identical to that described previously, with an iterative solution converging on the final values of $\tilde{U}_{j,k}$ and $\tilde{x}_{j,k}$ ($j = 1, 2, \ldots, N$). Equation (6.6) provides the initial guesses, which are alternatingly improved by (6.7) and by (6.10), (6.1), (6.2). Following convergence, $\Delta\tilde{t}_k$ is either doubled, unchanged or halved (with the time-step calculation retried in the latter case), depending on the estimated magnitude of the relative discretization error. Even with this step-wise optimization, however, the matrix equation was solved 1000–5000 times during the $\tilde{\rho} - 1 \ll 1$ experiments, requiring 10–45 s of I.B.M. 370/168 computing time for three-sphere chains.

One notes that as $\mathrm{Re}_\infty \to 0$, the integration procedure for (4.1) reduces to that for (4.3), since clearly (6.10) reduces to (6.4) as the Reynolds number vanishes, thus providing a proper limit behaviour in which the short time scale of the initial acceleration period has been shrunk to zero.

7. Results for three coaxial free falling spheres

In this section, the numerical results will be presented for three-sphere chains under a variety of Reynolds numbers and initial configurations. The initial spacings considered vary in the range $1 \leqslant \tilde{b}_0 \leqslant 10$ and $1 \leqslant \tilde{c}_0 \leqslant 10$, where

$$\tilde{b}_0 = \tilde{b}(0), \qquad \tilde{c}_0 = \tilde{c}(0),$$
$$\tilde{b}(t) = b(t)/a, \qquad \tilde{c}(t) = c(t)/a,$$

and b and c are centre-to-centre sphere spacings, defined in the insert of figure 7. Subsection (a) describes the critical spacing condition for the near collision approach of three settling spheres. Subsection (b) compares the predictions of the $\mathrm{Re}_\infty = 0$ and $\mathrm{Re}_\infty \ll 1$ theory with the experimental data obtained from a typical three sphere experiment using the low Reynolds number settling apparatus described below. The effects of unsteady inertial forces are presented in subsection (c) in conjunction with the results of the $0 < \mathrm{Re}_\infty \ll 1$ runs.

While the numerical experiments presented herein corroborate the qualitative observations reported in Happel & Pfeffer (1960), there are no existing data to compare with the theory's quantitative predictions. For this reason, the authors have constructed a low Reynolds number settling apparatus for the purpose of obtaining detailed measurements in which unsteady inertial

effects could be documented. The apparatus consisted of a 2 m, clear, rigid cylinder with a constant diameter of 50 cm, which was filled with a highly viscous liquid (viscosity 18.5 g cm^{-1} s^{-1}, relative density 1.06). Small, identical, plastic spheres (relative density 1.147, diameter 0.905 cm) were released coaxially into the fluid. Accurate measurements of the particle trajectories as functions of time were made from large-scale projections of the filmed runs, taken at known regular intervals.

(*a*) *Critical-spacing criterion for near-approach of spheres*

The qualitative behaviour of three coaxial spheres falling at low Reynolds number was described in § 1 for the case where spheres 2 and 3 asymptotically approach collision as illustrated in figure 1. In simulating this behaviour in the numerical experiments a program-termination condition had to be incorporated, taking into account the breakdown of the multipole truncation procedure as the gap width goes to zero, as discussed in § 5. With figure 6 as a guide, an effective collision was understood to have occurred if spheres 2 and 3 had approached to within a gap of 0.05 diameters and had a finite relative velocity which, if extrapolated, would have taken the spheres through the contact condition $\tilde{c} = 1$. When this occurred it was understood that the limit had been reached and that the relative velocity $\tilde{U}_2 - \tilde{U}_3$ will asymptote rapidly to zero.

In other numerical experiments, however, the relative velocity $\tilde{U}_2 - \tilde{U}_3$ vanished before the effective collision distance $\tilde{c} = 1.05$ was obtained. In these situations one found that spheres 2 and 3 asymptotically approached a finite gap, while sphere 1 was already too far behind to have any appreciable interaction with them. The unequal interactions which sphere 1 has with the other two spheres causes sphere 2 to settle faster than sphere 3, but as the 2–3 doublet moves away from sphere 1, the relative velocity, $\tilde{U}_R \equiv \tilde{U}_2 - \tilde{U}_3$, decreases monotonically. One, therefore, suspects, based on the following consideration of the two extreme cases $\tilde{b}_0 = 1$ and $\tilde{b}_0 \to \infty$, that there is a critical configuration condition which determines whether for a specified $\tilde{c}_0$ an effective collision between the two lead spheres will be achieved.

In the case of spheres 1 and 2 initially touching ($\tilde{b}_0 = 1$), sphere 2 will always close its gap with sphere 3, regardless of the initial spacing $\tilde{c}_0$. Even for an arbitrarily large $\tilde{c}_0$, spheres 1 and 2 can settle as an isolated doublet for as long as is necessary to approach and fall under the influence of sphere 3. On the other hand, if sphere 1 is initially very far away from sphere 2 ($\tilde{b}_0 \to \infty$), the 2–3 doublet will forever be isolated and settle with $\tilde{U}_3 = \tilde{U}_2 > \tilde{U}_1$. We conclude, therefore, that for any initial spacing $\tilde{c}_0$ there must exist some critical initial spacing $\tilde{b}_0 = \tilde{b}_{\mathrm{cr}}$, such that when $\tilde{b}_0 < \tilde{b}_{\mathrm{cr}}$ the lubrication limit would be reached, and when $\tilde{b}_0 > \tilde{b}_{\mathrm{cr}}$ the relative velocity $\tilde{U}_R$ would vanish with the inter-particle gap still open.

Accordingly, a series of numerical experiments was conducted to determine $\tilde{b}_{\mathrm{cr}}(\tilde{c}_0)$. The results are tabulated in table 1 and are plotted in figure 7 for $\tilde{\rho} = 1.1$ and $\mathrm{Re}_\infty = 0.1$ and 0. Any combination of initial spacings located under the curve will result in a 'near' collision.

TABLE 1. VALUES OF CRITICAL SPACING $\tilde{b}_{\mathrm{cr}}$ FOR $\tilde{\rho} = 1.1$

$\tilde{c}_0$	$\tilde{b}_{\mathrm{cr}}$ ($\mathrm{Re}_\infty = 0$)	$\tilde{b}_{\mathrm{cr}}$ ($\mathrm{Re}_\infty = 0.1$)
1.2	6.428	6.545
1.6	2.845	2.995
2	2.102	2.273
3	1.553	1.659
4	1.355	1.470
7	1.170	1.301
10	1.113	1.246

PHILOSOPHICAL TRANSACTIONS OF THE ROYAL SOCIETY A MATHEMATICAL, PHYSICAL & ENGINEERING SCIENCES

(b) Comparison of theoretical and experimental results

As mentioned earlier in this section, experimental data were collected for the time-dependent settling of three coaxial spheres. The data for a typical run $\mathrm{Re}_\infty = 0.011$, $\tilde{\rho} = 1.08$, $\tilde{b}_0 = 1.63$, and $\tilde{c}_0 = 7.38$ are compared with the theoretical predictions in figure 8. The agreement between theory and experiment was found to be excellent provided the unsteady forces are retained in equation (4.1). One also observes in figure 8 that the solution curve based on the full equation (4.1) is virtually indistinguishable from the one obtained when the only unsteady force retained

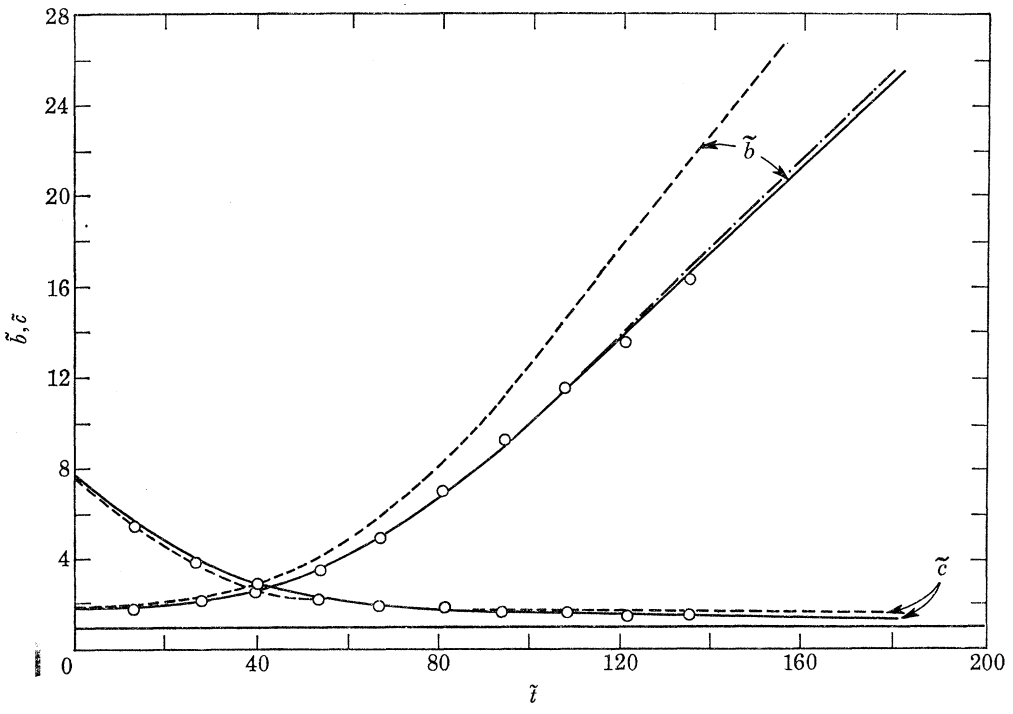

FIGURE 8. Comparison of theory with experimental data on sphere spacings; $\tilde{b}_0 = 1.63$, $\tilde{c}_0 = 7.38$. ——, $\mathrm{Re}_\infty = 0.011$, $\tilde{\rho} = 1.08$ theory, all forces. ·—·—, $\mathrm{Re}_\infty = 0.011$, $\tilde{\rho} = 1.08$ theory, Basset force only. – – –, $\mathrm{Re}_\infty = 0$ theory. ○, Experimental data.

in equation (4.1) is the Basset force. In contrast, the $\mathrm{Re}_\infty = 0$ theory based on equations (4.3) and (4.4), in which all unsteady forces are neglected, leads to discrepancies which progressively increase with time. The maximum deviation between theory and experiment when the Basset force effect is included is 2.9 %.†

At first glance, it is somewhat surprising that the presence of the Basset force for large times $\tilde{t} > 80$ leads to a difference in sphere spacing $\tilde{b}$ in figure 8 which is of $O(1)$ or larger compared to the sphere dimensions when the velocity difference due to the Basset force decays as $\tilde{t}^{-\frac{1}{2}}$. This basic behaviour can be deduced from the following approximate analysis. For large times the virtual mass and acceleration forces can be neglected to $O(\mathrm{Re}_\infty^{\frac{1}{2}})$ with the result that equation (4.1) reduces to

$$\tilde{U}_j = \frac{1}{\lambda_j} - \frac{1}{\lambda_j}\frac{\mathrm{Re}_\infty^{\frac{1}{2}}}{\sqrt{(2\pi)}}\int_0^{\tilde{t}} \frac{\mathrm{d}\tilde{U}_j}{\mathrm{d}\tilde{\tau}}\frac{\mathrm{d}\tilde{\tau}}{\sqrt{(\tilde{t}-\tilde{\tau})}}. \tag{7.1}$$

† Based on the theory presented in Leichtberg, Pfeffer & Weinbaum (1976*a*), the wall correction factors are 1.057 on the central sphere and 1.069 on the outer ones. The pertinent quantity for figure 8 is their difference, 1.2 %, which was neglected.

Inserting this result into the expression $\mathrm{d}\tilde{b}/\mathrm{d}\tilde{t} = \frac{1}{2}(\tilde{U}_2 - \tilde{U}_1)$ for the time rate of change of the spacing between spheres 1 and 2, one obtains

$$2\frac{\mathrm{d}\tilde{b}}{\mathrm{d}\tilde{t}} = \frac{\lambda_1 - \lambda_2}{\lambda_1\lambda_2} + \frac{\mathrm{Re}_\infty^{\frac{1}{2}}}{2\pi}\int_0^{\tilde{t}}\left(\frac{1}{\lambda_1}\frac{\mathrm{d}\tilde{U}_1}{\mathrm{d}\tilde{\tau}} - \frac{1}{\lambda_2}\frac{\mathrm{d}\tilde{U}_2}{\mathrm{d}\tilde{\tau}}\right)\frac{\mathrm{d}\tilde{\tau}}{\sqrt{(\tilde{t}-\tilde{\tau})}}. \tag{7.2}$$

If the period of the initial rapid acceleration $\tilde{t}_s$ is short compared to the current time $\tilde{t}$ (the upper limit of the integral in (7.2)) and the contribution of the small accelerations to the Basset force integral for times larger than $\tilde{t}_s$ are neglected, equation (7.2) can be approximated by

$$2\frac{\mathrm{d}\tilde{b}}{\mathrm{d}\tilde{t}} = \frac{\lambda_1 - \lambda_2}{\lambda_1\lambda_2} + \frac{1}{\sqrt{(2\pi)}}\left(\frac{\mathrm{Re}_\infty}{\tilde{t}}\right)^{\frac{1}{2}}\left(\frac{\tilde{U}_{1s}}{\lambda_1} - \frac{\tilde{U}_{2s}}{\lambda_2}\right), \tag{7.3}$$

where $\tilde{U}_{1s}$ and $\tilde{U}_{2s}$ are the sphere velocities at time $\tilde{t}_s$. For $\tilde{t} \gg 1$, two important results are readily deduced from equation (7.3). First, the integral of the Stokes drag term increases nearly linearly with time (note that the curve for $\mathrm{Re}_\infty = 0$ is nearly linear for $\tilde{t} > 80$ in figure 8), since the λ_j are changing very slowly for these large times. Second, the velocity difference due to the second term on the right hand side of equation (7.3) is of $O(\mathrm{Re}_\infty/\tilde{t})^{\frac{1}{2}}$ and thus of $O(\mathrm{Re}_\infty)$ when $\tilde{t}$ is of $O(\mathrm{Re}_\infty^{-1})$, the time period where the sizeable differences between the $\mathrm{Re}_\infty = 0$ theory and the experimental data are observed in figure 8. The velocity difference due to this term is of $O(10^{-2})$ and thus too small to account for the observed velocity differences. The unexpectedly large deviation from the $\mathrm{Re}_\infty = 0$ theory results is due to the important effect of the Basset force on the λ_j factors in the first term on the right hand side of equation (7.3). As will be discussed later in connection with table 2 and figure 11, the Basset force has an important influence on the relative velocity difference of the spheres in the intermediate time period $O(\mathrm{Re}_\infty) < \tilde{t} \leqslant O(10^2\,\mathrm{Re}_\infty)$ between the decay of the virtual mass and inertial forces and the establishment of the long time quasi-steady behaviour. The integrated effect of the Basset force during this intermediate time interval produces a significant change in the U_j and hence the λ_j and is thus able to appreciably alter the long time trajectories of the spheres by changing the initial conditions for the long time scale transient motion.

(*c*) *Effects of unsteady forces at low Reynolds number*

The significant difference between the results of the $\mathrm{Re}_\infty = 0$ and the $0 < \mathrm{Re}_\infty \ll 1$ theoretical predictions and the close agreement between the experimental data and the theory for the full equation (4.1), as illustrated in figure 8, strongly motivate a more detailed numerical study of the contributions of the various unsteady forces at low Re_∞ on both the short and long time scales.

Figures 9 and 10 are velocity–time profiles for each sphere in a typical numerical experiment which leads to near collision, $\tilde{b}_0 \approx 1$, $\tilde{c}_0 = 10$, $\tilde{\rho} = 1.1$ at $\mathrm{Re}_\infty = 0$ and $\mathrm{Re}_\infty = 0.1$. After the initial unsteady period (which is shrunk to zero at $\mathrm{Re}_\infty = 0$, figure 9), spheres 1 and 2 possess essentially the same velocities, which are 30–40 % greater than the velocity of sphere 3.† The velocity of sphere 2 does not vary greatly from this point to the end of the experiment. Sphere 3, however begins to accelerate due to the reduction in its drag created by the approach of the doublet consisting of spheres 1 and 2. At the same time sphere 1 begins to decelerate due to the decrease in the drag reduction effect produced by sphere 2 separating and moving away from it.

At some point in time, spheres 1 and 3 will have the same velocity, indicating that the spacing parameters $\tilde{b}$ and $\tilde{c}$ are equal. From that point on the velocities of spheres 2 and 3 will approach

† Note spheres 1 and 2 will not separate if $\tilde{b}_0$ is identically unity since this problem is the inverse of the near collision problem for spheres 2 and 3 treated in § 5. Spheres 1 and 2 are then started from an effective touching condition with $\tilde{b}_0 = 1+\epsilon$, where $\epsilon \ll 1$.

PHILOSOPHICAL TRANSACTIONS OF THE ROYAL SOCIETY A MATHEMATICAL, PHYSICAL & ENGINEERING SCIENCES

each other while that of sphere 1 will decrease and asymptote to a value of $U_1/U_t = 1.0$, i.e. the terminal settling velocity of a single isolated sphere. The relative velocity curves,

$$\tilde{U}_{2,3}(\tilde{t}) = \tilde{U}_2(\tilde{t}) - \tilde{U}_3(\tilde{t}) \quad \text{and} \quad \tilde{U}_{1,2}(\tilde{t}) = \tilde{U}_2(\tilde{t}) - \tilde{U}_1(\tilde{t}),$$

are shown in figure 11 for the same runs and also for $\mathrm{Re}_\infty = 0.01$.

Figures 9 to 11 reveal that the practical effect of the unsteady terms in equation (4.1) is to reduce the relative velocity $\tilde{U}_{1,2}$ and hence the spacing $\tilde{b}$ between spheres 1 and 2. This, in turn, increases the relative velocity of approach between spheres 2 and 3, as shown in figure 11, since the velocities of these two spheres are made unequal by their unequal interactions with sphere 1,

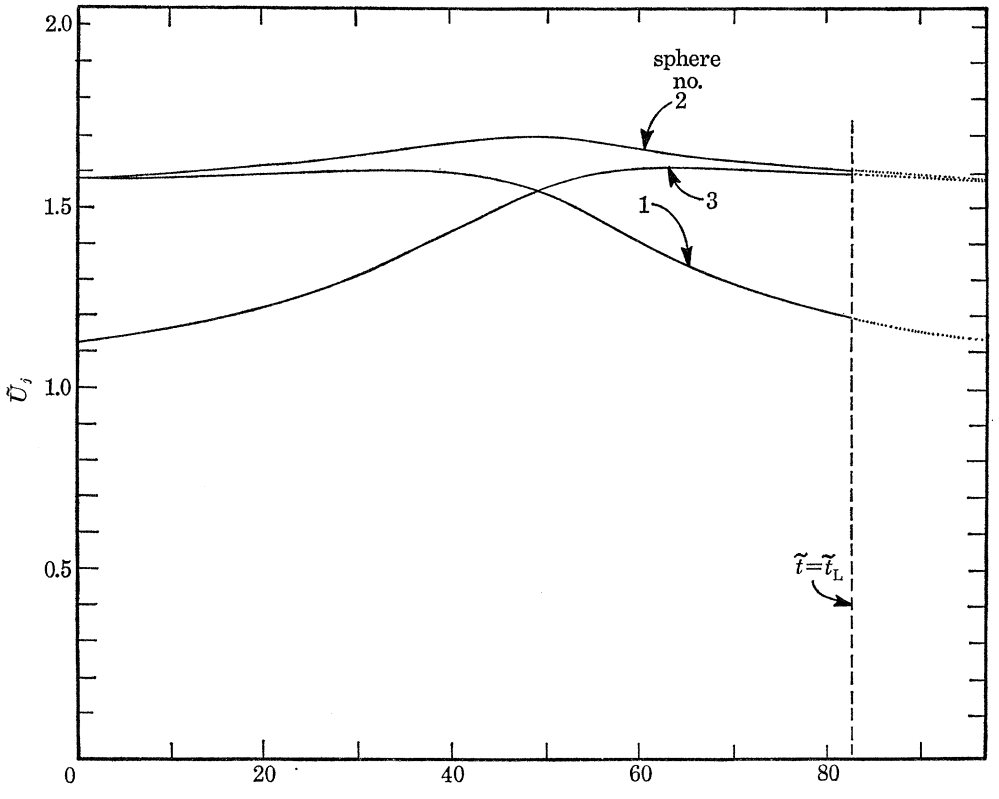

FIGURE 9. Velocity–time curves for a three-sphere chain, $\tilde{b}_0 \approx 1$, $\tilde{c}_0 = 10$, $\mathrm{Re}_\infty = 0$; $\tilde{t}_L$ is defined by $\tilde{c}(\tilde{t}_L) = 1.05$.

the strength of the interaction being approximately inversely proportional to the spacing. The lubrication limit between spheres 2 and 3 is, therefore, reached sooner (if $\tilde{b}_0 < \tilde{b}_{cr}$), as a result of including the unsteady and inertial forces. As expected from the foregoing discussion, the effect of the unsteady forces, which increases with the Reynolds number, on the critical spacing curve is a modest increase in $\tilde{b}_{cr}(\tilde{c}_0)$, as shown in figure 7.

Of particular interest relevant to our previous discussion of figure 8 is the relatively large difference in the relative velocity curves for the $\mathrm{Re}_\infty = 0$ and $\mathrm{Re}_\infty = 0.01$ cases observed in figure 11. The results for the $\mathrm{Re}_\infty = 0.1$ and $\mathrm{Re}_\infty = 0.01$ cases show that the approach to the initial quasi-steady settling velocity is roughly two orders of magnitude longer than the initial short time scale of $O(\mathrm{Re}_\infty)$ over which the sphere's inertia is important. A more detailed insight into this behaviour can be had by examining the relative magnitudes of the different unsteady

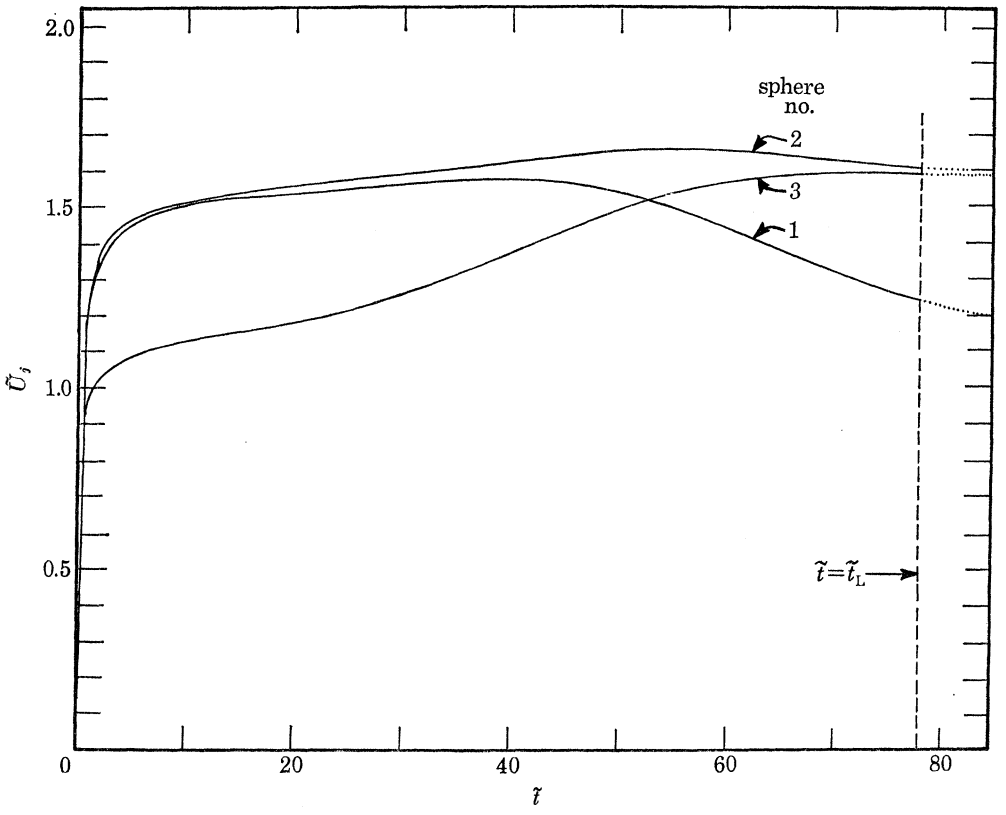

FIGURE 10. Velocity–time curves for a three-sphere chain, $\tilde{b}_0 \approx 1$, $\tilde{c}_0 = 10$, $\mathrm{Re}_\infty = 0.1$, $\tilde{\rho} = 1.1$.

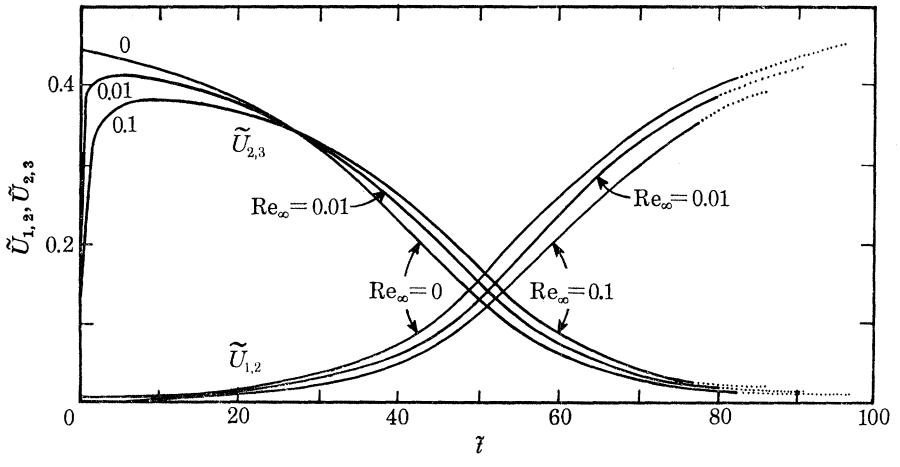

FIGURE 11. Relative velocity plotted against time for the two leading and trailing spheres of a three-sphere chain, $\tilde{b}_0 \approx 1$, $\tilde{c}_0 = 10$, $\tilde{\rho} = 1.1$, $\mathrm{Re}_\infty = 0.1$, 0.01 and 0.

forces acting on the three sphere system at different times in typical numerical experiments at several values of Re_∞. Such data are presented in table 2, where we have calculated the ratio of each of the unsteady forces to the buoyancy force B at different times for the case $\tilde{b}_0 \approx 1$, $\tilde{c}_0 = 10$, $\tilde{\rho} = 1.1$ at $\mathrm{Re}_\infty = 0.1$ and 0.01 for each of the three spheres. Equation (4.1) can be written in terms of these force ratios as

$$\frac{F_{\mathrm{d.}}}{B} + (2\tilde{\rho}+1)\frac{F_{\mathrm{v.m.}}}{B} + \frac{F_{\mathrm{B}}}{B} = 1. \tag{7.4}$$

One concludes from table 2 that the virtual mass and inertial forces have decayed to less than 2 % of the buoyancy force when $\tilde{t} = \mathrm{Re}_\infty$ while the Basset force at this time is of comparable magnitude to both the buoyancy and Stokes drag forces. The instantaneous velocity of the spheres at $\tilde{t} = \mathrm{Re}_\infty$ is roughly a half of their initial quasi-steady settling velocity. The Basset force is thus by far the most important unsteady force governing the transition to the long time scale transient motion. The exact magnitude of the Basset force depends on the integrated time history of the acceleration of each sphere and retains its significance a long time after the initial rapid acceleration has died out. For example, the results in table 2 show that F_B/B for spheres 1 and 2 is approximately 0.19, 0.06 and 0.02 at $t = 10\,\mathrm{Re}_\infty$, $100\,\mathrm{Re}_\infty$ and $1000\,\mathrm{Re}_\infty$ respectively. It is this slow decay of the initial transient motion due to the Basset force and its effect on the instantaneous values of the λ_j that produces the unexpectedly large deviations from the $\mathrm{Re}_\infty = 0$ theory results observed in figures 8–11.

TABLE 2. FORCES ACTING ON THE THREE SPHERE SYSTEM FOR $\tilde{\rho} = 1.1$, $\tilde{b}_0 \approx 1$, $\tilde{c}_0 = 10$

		$F_{d.}/B$			$F_{v.m.}/B$			F_B/B		
Re_∞	$\tilde{t}$	sphere 1	sphere 2	sphere 3	sphere 1	sphere 2	sphere 3	sphere 1	sphere 2	sphere 3
0.1	0.001	0.026	0.025	0.037	2.05×10^{-1}	2.05×10^{-1}	2.02×10^{-1}	0.318	0.319	0.317
	0.01	0.154	0.152	0.213	9.45×10^{-2}	9.48×10^{-2}	8.60×10^{-2}	0.544	0.545	0.512
	0.1	0.492	0.490	0.594	1.55×10^{-2}	1.56×10^{-2}	1.08×10^{-2}	0.458	0.460	0.371
	1	0.807	0.806	0.858	8.02×10^{-4}	8.05×10^{-4}	4.68×10^{-4}	0.190	0.191	0.140
	10	0.937	0.936	0.952	3.33×10^{-5}	3.51×10^{-5}	3.44×10^{-5}	0.063	0.064	0.048
	70	0.989	0.976	0.971	-5.95×10^{-5}	-1.42×10^{-5}	-2.59×10^{-6}	0.011	0.024	0.029
0.01	0.0001	0.026	0.025	0.037	2.05×10^{-1}	2.05×10^{-1}	2.05×10^{-1}	0.318	0.319	0.317
	0.001	0.154	0.152	0.213	9.45×10^{-2}	9.48×10^{-2}	8.60×10^{-2}	0.544	0.545	0.512
	0.01	0.494	0.492	0.596	1.53×10^{-2}	1.54×10^{-2}	1.07×10^{-2}	0.457	0.459	0.369
	0.1	0.807	0.806	0.858	8.00×10^{-4}	8.03×10^{-4}	4.60×10^{-4}	0.190	0.191	0.140
	1	0.937	0.937	0.954	2.93×10^{-5}	2.95×10^{-5}	1.75×10^{-5}	0.063	0.063	0.046
	10	0.980	0.980	0.985	1.47×10^{-6}	1.68×10^{-6}	2.73×10^{-6}	0.020	0.020	0.015
	70	0.997	0.993	0.991	-5.63×10^{-6}	-1.65×10^{-6}	-4.02×10^{-7}	0.003	0.007	0.009

TABLE 3. SHORT AND LONG TIME SCALE BEHAVIOUR, $\tilde{b}_0 \approx 1$, $\tilde{c}_0 = 10$, $\tilde{\rho} = 1.1$

Re_∞	$\tilde{t}_s$	$\tilde{t}_L$	$2\tilde{b}(\tilde{t}_L)$
10^{-1}	1.36×10^{-1}	78.7	10.24
10^{-2}	1.43×10^{-2}	80.6	12.32
10^{-4}	1.37×10^{-4}	82.4	13.62
0	–	82.6	13.78

Table 3 provides further interesting data, regarding the two-time-scale motion of the spheres, for the $\tilde{b}_0 \approx 1$, $\tilde{c}_0 = 10$, $\tilde{\rho} = 1.1$ case at four different Reynolds numbers. Listed are values of (*a*) $\tilde{t}_s$, the duration of the initial acceleration period in the long time coordinate, defined as that point in time when the virtual mass force decays to less than 1 % of the buoyancy force; (*b*) $\tilde{t}_L$, the time required for sphere 2 to approach sphere 3 to within 0.05 diameters ($\tilde{c} = 1.05$) and (*c*) the separation distance $2\tilde{b}(\tilde{t}_L)$ between spheres 1 and 2 at this time, given by

$$2\tilde{b}(\tilde{t}_L) = 2 + \int_0^{\tilde{t}_L} (\tilde{U}_2 - \tilde{U}_1)\,\mathrm{d}\tilde{t}.$$

The effect of increasing Re_∞ is to decrease both $\tilde{t}_L$ and $\tilde{b}(\tilde{t}_L)$. Particularly striking are the large changes in sphere spacing that result over an extended run due to the accumulated effect of the Basset forces discussed in connection with figure 8. One also observes in table 3 that the virtual

mass force decays to less than 1 % of the buoyancy force when $\tilde{t} \approx 1.4\,\mathrm{Re}_\infty$. Thus, in terms of the short time variable t^*, $t_s^* \approx 1.4$ independent of Re_∞.

In concluding this section, we shall take note of the consequences of the reversible nature of a purely Stokes flow, i.e. $\mathrm{Re}_\infty = 0$. Figure 12 presents the $\tilde{b}(\tilde{t})$ and $\tilde{c}(\tilde{t})$ curves for the $\tilde{b}_0 \approx 1$, $\tilde{c}_0 = 10$, $\tilde{\rho} = 1.1$ case at two Reynolds numbers, $\mathrm{Re}_\infty = 0.1$ and 0. These curves, like all previous time plots, terminate at $\tilde{t} = \tilde{t}_L$, defined by $\tilde{c}(\tilde{t}_L) = 1.05$. Figures 9–12, however, have been extended (dotted lines) to include the extrapolated sphere motion as predicted by the present truncation method following the onset of lubrication-limit forces for $\tilde{c}(\tilde{t}) \leqslant 1.05$.

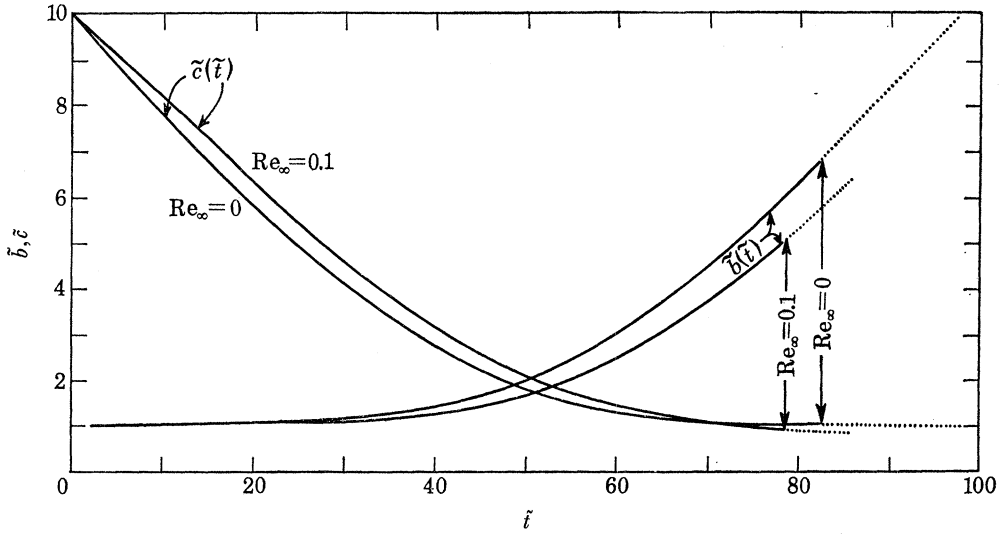

FIGURE 12. Sphere spacings plotted against time for a three-sphere chain, $\tilde{b}_0 \approx 1$, $\tilde{c}_0 = 10$, $\tilde{\rho} = 1.1$, $\mathrm{Re}_\infty = 0.1$ and 0.

A striking feature of the two $\mathrm{Re}_\infty = 0$ spacing curves of figure 12 is the symmetry which exists about the half-time point, $\tilde{t} = 48.7$. The same symmetry exists for the three $\mathrm{Re}_\infty = 0$ velocity curves in figure 9. Thus, at $\mathrm{Re}_\infty = 0$, the second half of the experiment is an identical duplicate of the first half, in reverse. This phenomenon of reciprocity in the spheres' behaviour at zero Reynolds number is due to the absolute reversibility of Stokes flow in the absence of unsteady inertial forces. This non-directional nature of a pure Stokes flow also explains why two identical objects settling as an isolated doublet have identical velocities, despite the fact that one is leading and the other trailing. At non-zero Reynolds numbers, the reciprocity no longer exists because of the unsteady forces, as observed for the $\mathrm{Re}_\infty = 0.1$ curves in figure 12.

The reciprocity principle was used as a check on the over-all accuracy of the numerical procedures by conducting the $\tilde{b}_0 \approx 1$ numerical experiment at $\mathrm{Re}_\infty = 0$ and checking for compliance with the reciprocal terminal condition $\tilde{b} = \tilde{c}_0$. It was found that the total accumulated error at the end of a run was 0.40 %, 0.13 % and 0.06 % for $\tilde{c}_0 = 20$, 10, and 5, respectively.

8. Results for chains of more than three spheres

Numerical runs were conducted for chains of 4–25 settling spheres, using the theory and the numerical procedures developed in §§ 2–6. These runs showed a behaviour pattern for long chain which strongly suggested that chains of non-touching spheres will generally tend to break up into

smaller groups. While the question of instability to lateral disturbances has not been carefully examined at this time, the authors have observed the coaxial settling of as many as seven spheres in the experimental apparatus described at the beginning of § 7.

Consider a chain of N spheres, $N > 3$, equally spaced at $t = 0$, indexed from the trailing sphere ($j = 1$) to the leading sphere ($j = N$). Consider, too, as an accompanying example, figure 13, which plots the time-dependent inter-sphere spacings $\tilde{D}_{j,j+1}(\tilde{t})$ ($j = 1, \ldots, 6$) for a seven-sphere chain at $\mathrm{Re}_\infty = 0$ with an equal initial sphere spacing $\tilde{D}_{j,j+1}(0) = 2$. In the initial equally spaced configuration, the settling velocity is greatest for the central sphere, and decreases progressively toward the ends of the chain. This neat ordering of the sphere velocities can degenerate when the spacings are unequal, since a central sphere may settle more slowly than a non-central one if the former is more isolated from its neighbours. However, for any configuration, the outer spheres $j = 1$ and $j = N$ necessarily experience less interaction than their immediate neighbours, $j = 2$ and $j = N-1$. Hence, $U_2 > U_1$ and $U_{N-1} > U_N$. As a result, the spacing between spheres 1 and 2, D_{12}, is monotonically increasing as sphere 1 becomes more isolated, while the spacing between spheres $N-1$ and N, $D_{N-1,N}$, continually decreases until the gap is nearly closed and spheres $N-1$ and N move as a steady doublet.

By this time, the spacing D_{12} has increased sufficiently to render sphere 1 fairly isolated, while the other spacings, $D_{23}, D_{34}, \ldots, D_{N-2,N-1}$, have changed by smaller amounts. The problem is now transformed to one of a chain of $N-1$ interacting spheres headed by a doublet and followed by a single, increasingly isolated sphere. Sphere 2 will now fall further behind, since it is now effectively the trailing sphere of the chain. At the leading end of the chain the behaviour depends on the spacings, as follows. If the spacing is such that U_{N-2} exceeds the velocity of the $N-(N-1)$ doublet, then the spacing $D_{N-2,N-1}$ decreases steadily until a triplet is formed. If, on the other hand, the doublet's velocity exceeds U_{N-2}, the doublet will move further ahead of the rest of the chain until the doublet is nearly isolated. At this point spheres $N-2$ and $N-3$ start behaving like the leading spheres of an $N-3$ sphere chain, forming a doublet, and the cycle of events continues.

The numerical experiments were not carried beyond this point due to computer time limitations, but the general pattern of the spheres' behaviour is evident. The trailing third of a long chain of spheres will disintegrate into a series of single, isolated spheres. The leading half to two-thirds of the chain will break up into a series of doublets and triplets which, extrapolating the pattern of behaviour for very long chains, would then recombine to form a series of short unsteady chains.

Figure 13 illustrates the long chain behaviour discussed above for the time period $0 \leqslant \tilde{t} \leqslant 30$. The spacing $\tilde{D}_{67}$ was artificially constrained to remain constant at 1.05 diameters after the gap narrowed to this lubrication limit.

9. Related work and concluding remarks

The problem of the creeping motion of a finite chain of spheres in a cylindrically bounded medium has also been solved by the authors using similar procedures to those described herein and is currently being prepared for publication, Leichtberg *et al.* (1976*a*). This latter work is being used as the basis for a theoretical study of a possible hydrodynamic mechanism for the formation of rouleaux in the microcirculation (1976*b*). We have also been interested in the behaviour of the three sphere problem for values of Re_∞ in the transition region where the length of the short time scale $\tilde{t}_s$ is of $O(1)$ or larger. An approximate semi-analytic theory was, therefore, developed for

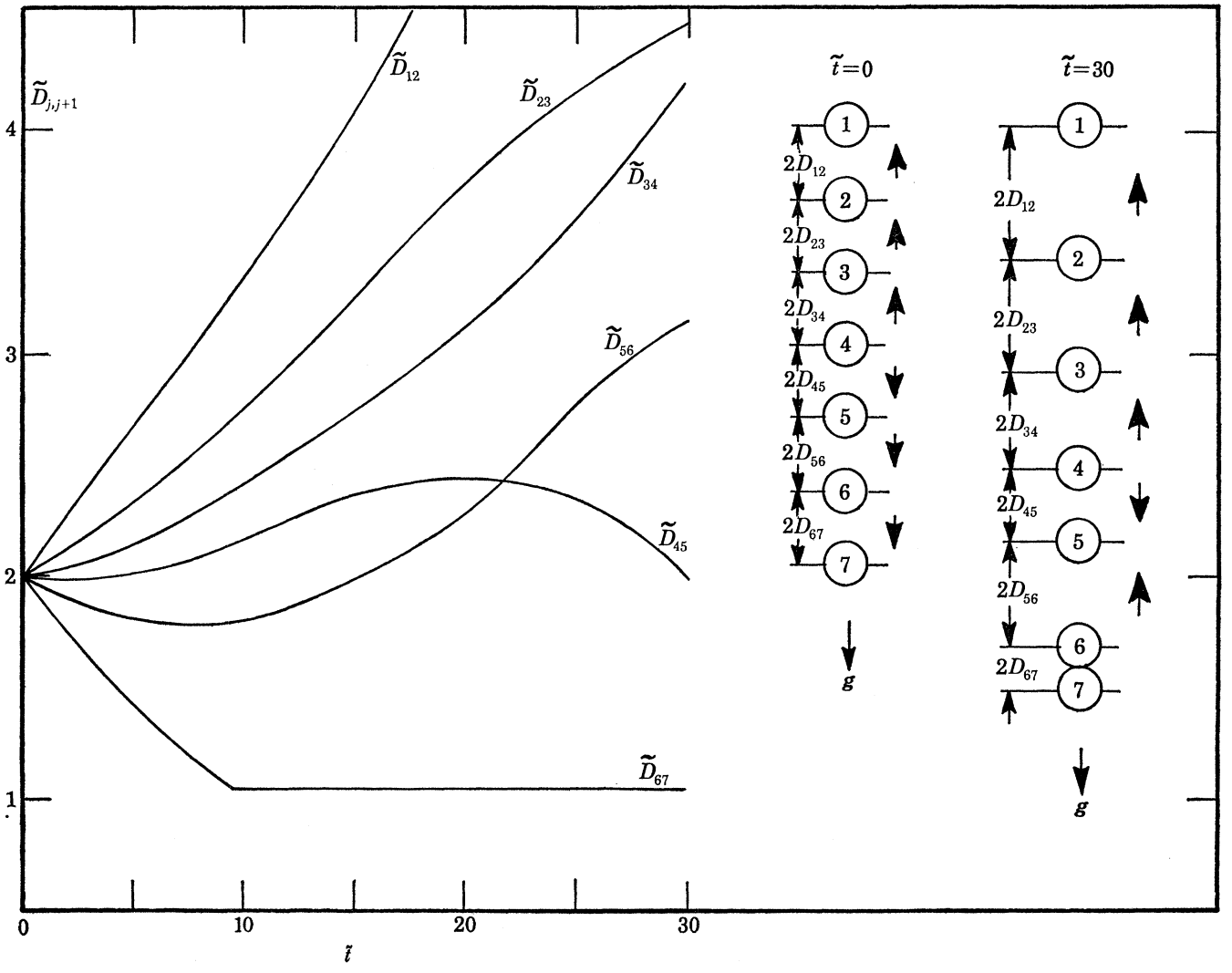

FIGURE 13. Sphere spacings plotted against time for a seven-sphere chain. $\tilde{D}_{j,j+1}(0) = 2$ $(j = 1, 2, \ldots, 6)$, $\mathrm{Re}_\infty = 0$; ↑, spacing is increasing; ↓, spacing is decreasing.

the Reynolds number range $1 < \mathrm{Re}_\infty < 10$ where convective inertial effects are important but incipient wake bubble formation has not yet occurred. This study has been completed and will be reported elsewhere (Gluckman, Pfeffer & Weinbaum, 1976).

The most interesting new result of the investigation, which would appear to be of general validity for all multiparticle gravitational–Stokes flow interactions, is the importance of the Basset force in flow configurations which are slowly changing due to particle interactions. The theoretical and experimental results for the simple three-sphere geometry treated herein clearly show that departures of $O(1)$ from zero Reynolds number theory will result due to the cumulative effect of the Basset force, when the particle Reynolds number $2aU_t/\nu$ based on its terminal settling velocity U_t is $\ll 1$ but the duration of the interaction is of $O(\mathrm{Re}_\infty^{-1} a/U_t)$ or longer. Since particles in sedimenting flows usually travel many diameters before approaching boundaries, the above condition is encountered in most applications. Virtual mass and particle acceleration forces, on the other hand, are very short lived and in many applications can be neglected entirely. The

results also indicate that both the virtual mass and Basset forces are not significantly altered by multiparticle interaction effects and are thus adequately approximated by their single particle representations for most engineering purposes.

The numerical results obtained in this study demonstrate that it is feasible with the present generation of computers to examine the fluid–particle interaction between moderate numbers of geometrically simple objects, provided a rapidly converging numerical technique can be devised for calculating the instantaneous quasi-steady state drag on each object. The multipole truncation technique developed in Gluckman *et al.* (1971) was well suited to this objective for the axisymmetric flow past spheres and spheroids. More than 10^4 quasi-steady three-sphere interactions with drag results accurate to better than 0.1 % could be obtained in less than a minute on a moderate capacity present generation computer by means of this technique. The extension of this technique to truncated spherical harmonic representations of arbitrary three-dimensional multiple sphere configurations is currently in progress.

This research was supported by National Science Foundation Grant no. GK-40802.

References

Bart, E. 1959 MCh.E. thesis. New York University.
Basset, A. B. 1888 *Hydrodynamics*. Cambridge: Deighton Bell. New York: Dover (1961).
Brenner, H. 1961 *Chem. Engng Sci.* **16**, 242.
Darwin, C. 1953 *Proc. Camb. Phil. Soc.* **49**, 342.
Gluckman, M. J., Pfeffer, R. & Weinbaum, S. 1971 *J. Fluid Mech.* **50**, 705.
Gluckman, M. J., Pfeffer, R. & Weinbaum, S. 1976 (to be published).
Gluckman, M. J., Weinbaum, S. & Pfeffer, R. 1972 *J. Fluid Mech.* **55**, 677.
Happel, J. & Pfeffer, R. 1960 *A.I.Ch.E. Jl* **6**, 129.
Hocking, L. M. 1964 *J. Fluid Mech.* **20**, 129.
Landau, L. D. & Lifshitz, E. M. 1959 Course of theoretical physics. In *Advanced physics*, vol. 6. New York: Addison-Wesley.
Leichtberg, S., Pfeffer, R. & Weinbaum, S. 1976*a* Stokes flow past finite coaxial clusters of spheres in a circular cylinder *Int. J. Multiphase Flow* (in the press).
Leichtberg, S., Weinbaum, S. & Pfeffer, R. 1976*b* A theory for the coaxial slow viscous motion of finite clusters of spheres in unbounded Poiseuille flow and its application to Rouleaux formation. *Biorheology* **13**, 165.
Milne-Thomson, L. M. 1960 *Theoretical hydrodynamics*, 4th ed. McMillan.
Skalak, R., Chen, P. H. & Chien, S. 1972 *Biorheology* **9**, 67.
Smoluchowski, M. 1911 *Bull. Int. Acad. Polonaise Sci. Lett.* 1 A.
Stimson, M. & Jeffery, G. B. 1926 *Proc. R. Soc. Lond.* A **111**, 110.
Wacholder, E. & Sather, N. F. 1974 *J. Fluid Mech.* **65**, 417.

PHILOSOPHICAL TRANSACTIONS OF THE ROYAL SOCIETY A MATHEMATICAL, PHYSICAL & ENGINEERING SCIENCES